

**Possible Mechanisms for Tsunami-like Surge Deposits  
Due to the Chicxulub Impact at the K-Pg Boundary at  
the Tanis Site, North Dakota**

Randall J. LeVeque, Department of Applied Mathematics, University of Washington, Seattle, USA, [rjl@uw.edu](mailto:rjl@uw.edu)

Robert A. DePalma, Department of Earth and Environmental Sciences, University of Manchester, UK, [paleogen@aol.com](mailto:paleogen@aol.com)

Carrie Garrison-Laney, Washington Sea Grant, University of Washington, Seattle, USA, [cegl@uw.edu](mailto:cegl@uw.edu)

Satish Maurya, Department of Earth Sciences, IIT Bombay, Mumbai, Maharashtra, India, [smaurya@iitb.ac.in](mailto:smaurya@iitb.ac.in)

Jan Smit, Department of Earth Sciences, Faculty of Science, Vrije Universiteit Amsterdam, Netherlands, [jansmit2@icloud.com](mailto:jansmit2@icloud.com)

Mark A. Richards, Department of Earth and Space Sciences, University of Washington, Seattle, USA [markrich@uw.edu](mailto:markrich@uw.edu)

---

This manuscript has been submitted for publication in the Journal of Geophysical Research (Solid Earth). Please note that, despite having gone through peer-review, the manuscript has yet to be formally accepted for publication. Subsequent versions of this manuscript may have slightly different content. If accepted, the final version of this manuscript will be available via the 'Peer-reviewed Publication DOI' link on the right-hand side of the EarthArxiv webpage for the paper.

---

Supplementary Information text is included in the pdf file and videos can be found at <https://faculty.washington.edu/rjl/pubs/ChicxulubTanisSurge/>

---

# Possible Mechanisms for Tsunami-like Surge Deposits Due to the Chicxulub Impact at the K-Pg Boundary at the Tanis Site, North Dakota

Randall J. LeVeque<sup>1</sup>, Robert A. DePalma<sup>2</sup>, Carrie Garrison-Laney<sup>3</sup>, Satish  
Maurya<sup>4</sup>, Jan Smit<sup>5</sup>, Mark A. Richards<sup>6</sup>

<sup>1</sup>Department of Applied Mathematics, University of Washington, Seattle, USA

<sup>2</sup>Department of Earth and Environmental Sciences, University of Manchester, UK

<sup>3</sup>Washington Sea Grant, University of Washington, Seattle, USA

<sup>4</sup>Department of Earth Sciences, IIT Bombay, Mumbai, Maharashtra, India

<sup>5</sup>Department of Earth Sciences, Faculty of Science, Vrije Universiteit Amsterdam, Netherlands.

<sup>6</sup>Department of Earth and Space Sciences, University of Washington, Seattle, USA

## Key Points:

- An ~10m surge event coincident with the Chicxulub impact transported mixed freshwater/marine organisms up the Tanis river valley.
- New modeling confirms limitations on the inland transport of marine fossils and helps to constrain the impact-related triggering mechanism.
- Other potential triggering mechanisms and strategic avenues of future study are discussed.

## Abstract

At Tanis, a unique bi-directional sediment package occurs precisely at the Cretaceous-Paleogene (KPg) boundary, recording the first hours of the Paleogene in uncommonly fine temporal detail. The impact ejecta-bearing sediment package was rapidly emplaced by two massive,  $\sim 10$ -meter-high, potentially impact-triggered surges, that inundated a steep, deeply incised paleo river valley from the direction of the contemporaneous Western Interior Seaway (WIS). Intermingling of fresh- and salt-water fossils at Tanis, coeval brackish water indicators in the nearby region, and historical tsunami observations, suggest that the WIS paleoshoreline was nearby Tanis at KPg time. The interpreted timing for deposition (including ejecta infall) of  $\sim 1$ -2-hours immediately post-impact precludes a direct tsunami from the Chicxulub impact site, which would have required much more than 10 hours to reach Tanis. Seismic waves from the Mw  $\sim 11$  Chicxulub earthquake, arriving just minutes post-impact, might have triggered the surge, for example, via seismic excitation of large water waves in the WIS, as proposed by DePalma et al. (2019). Here, we explore this mechanism via a simple mathematical model of seismic excitation and propagation of a water wave into a shallow river and upstream. Matching the observations implies a relatively long source process time of many minutes, such as generated by Chicxulub crater rebound processes, in order to explain sufficient upriver amplitudes and advective transport. Atmospheric waves due to the expanding Chicxulub ejecta curtain might have provided a smaller, secondary contribution during triggering. Thus, the mechanism(s) for the surges at Tanis are now better-constrained, yet remain incompletely resolved.

## Plain Language Summary

A remarkable geological record at the “Tanis” site (North Dakota) shows that two  $\sim 10$  meter high tsunami-like surges occurred on a point bar along a river upstream from the then existing Western Interior Seaway (WIS). The surge deposits are interpreted to have occurred within 1–2 hours of the Chicxulub impact associated with the end-Cretaceous mass extinction including the dinosaurs, and are challenging to explain via traditional tsunami mechanisms because they occurred too soon after the impact to have been tsunami waves traveling from the impact site. Alternative explanations include excitation of large water waves in the WIS due to seismic shaking from the magnitude  $\sim 11$  impact-generated earthquake or atmospheric effects from the expanding impact ejecta curtain. Here, we explore one potential triggering mechanism via a simple mathematical model of direct seismic excitation and propagation of a water wave into a shallow river and upstream. This model shows the difficulty of generating the observed surge deposits unless the timescale for impact-generated seismic waves is much longer than is commonly presumed. Thus the actual triggering mechanism(s) of the Tanis depositional surges remains incompletely resolved, while the sediment package bears a rich source of information about the global effects of the Chicxulub impact.

## 1 Introduction

A unique surge deposit at the Tanis site (North Dakota, USA) formed at exactly the K-Pg boundary, as recently described by DePalma et al. (2019, 2021). We summarize some key features but refer the reader to that paper for many more details and references that will not be repeated here. The surge deposit consists of a multi-unit sediment drape in the Hell Creek Formation that is 1.5 meters in thickness and deposited on the angled point-bar surface of a deeply incised paleo river that emptied into a body of seawater, presumably an arm of the Western Interior Seaway (WIS), and we refer to it as such below. The name and extent of this seawater body does not really matter for our investigations. The steep  $\sim 10.5$  meter isochronous elevation change from base to top of the point bar indicates that a 10 m amplitude surge would be required to deposit the

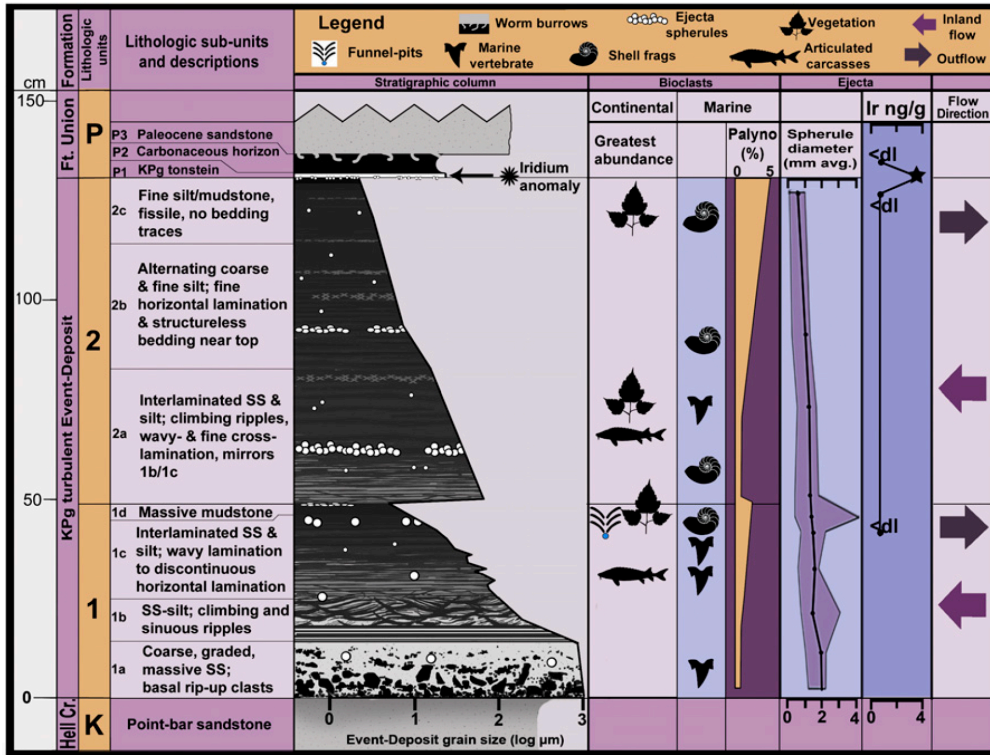


**Figure 1.** Tanis site stratigraphy and fossil distribution. Stratigraphic section of Tanis, outlining the lithological subdivisions and grain-size profile for the Event Deposit, abundance and primary stratigraphic distribution for a selection of continental and marine fossils, abundance of marine palynomorphs (palyno percentage), select impact-derived materials, and flow direction. (From DePalma et al. (2019), Figure 2.)

sediment package. The deposit is divided into two primary graded units representing two main *preserved* pulses of inflow and backwash (other smaller ones may have preceded these, but not have been sufficiently large or traveled sufficiently up-river to be preserved in the strata). As discussed by DePalma et al. (2019), the deposits are consistent with emplacement by massive long-period waves and are more similar to known tsunami deposits than to deposits left by short-period waves from severe storms.

The surge deposits contain impact ejecta spherules that are geochemically and geochronologically indistinguishable from ejecta from the Chicxulub impact (Yucatan Peninsula) at other locations, and are immediately overlain by an Ir-rich tonstein layer characteristic of K-Pg/Chicxulub impact deposits found worldwide (Bourgeois et al., 1988), providing a robust and precise temporal constraint for the site. The surge deposits contain contemporary freshwater (river-derived) and salt/brackish water (WIS-derived) fossils (Figure 1, "Bioclasts," indicating close proximity (likely just a few kilometers) of the point bar to the WIS. The surge deposits also contain freshwater fish fossils (paddlefish and sturgeons), whose body alignment indicates initial inland (westward) surges followed by water withdrawal eastward back toward the WIS. Remarkably about half of the paddlefish had ingested impact spherules from the river water column into their gill rakers, showing that they were buried alive by the surge deposits while impact spherules were still raining out of the air from the Chicxulub impact, and falling through the water column (Figure 1). Other evidence shows that, in very rare instances, relatively large (2–5 mm) diameter impact spherules landed upon the surface of the first surge deposit during a

short hiatus prior to arrival of the second major pulse. Thus it is clear that both surge deposits must have occurred within the  $\sim 1$ – $2$  hour time interval during which large spherules could have stayed aloft in ballistic trajectories through space and subsequent atmospheric re-entry at the  $\sim 3000$  km distance from Tanis to the impact site (Alvarez, 1996), whereas the overlying tonstein layer, consisting mostly of much finer dust particles, probably took many more hours to accumulate. The Tanis surge deposits therefore contain an almost stroboscopic record of the first few hours of the Paleogene, holding the potential for revealing details of the immediate aftermath of the Chicxulub impact at a global scale, its effects on continental biota, and the timing of its hazards in North America, which have proven elusive at other K-Pg boundary locations.

It is important to note that the precise timing of the infall of ejecta spherules is uncertain (see e.g., Artemieva and Morgan (2020) for a view contrasting with the scenario proposed by Alvarez (1996)), depending upon the physical processes that launched largely target-rock melt droplets from the Chicxulub impact, how this “ejecta curtain” propagated within and above the atmosphere, and the nature and duration of the settling process for their re-entry at the Tanis site. Nevertheless, the larger of these spherules are believed to have remained aloft no more than several hours in any case. We will return to this question in more detail later in this paper when we consider possible surge mechanisms associated with Chicxulub-induced atmospheric disturbances.

In addition to the invaluable utility of the sediment package and its fossil content, the emplacement mechanism for the deposit, itself, could provide further insight into the impact event and its effects. A key question regarding the nature of the Tanis deposit is that of how the two surges were generated. The surge package was anomalous for the Hell Creek Formation (HCF) (DePalma et al., 2019), both in depositional mode and fossil preservation, neither of which are yet known elsewhere in the HCF, and, regarding the close timing of the surge and impact, indicates that the two rare events likely bore a causative rather than just coincidental relationship. The timing of the surge as immediately post-impact, coinciding with the arrival of seismic waves from Chicxulub at the site, strongly suggests that the impact could have been a direct cause for the surges, i.e. via direct involvement such as direct excitation of water waves, or indirect involvement including triggering of mass-wasting (DePalma et al., 2019). The exact details of the triggering mechanism have not been fully explored or resolved beyond this basic hypothesis, and the aim of this study is to build upon that prior research by evaluating one of the multiple possible impact-related triggers for the Tanis surge deposit (direct excitation of waves) through mathematical modeling, and providing some preliminary commentary on other potential mechanisms that were not herein examined.

The sedimentology of the surge deposits is compatible with recent tsunami deposits (Engel et al., 2020), and quite similar to thick tsunami deposits found in many locations around the proto-Gulf of Mexico at K-Pg time (Bourgeois et al., 1988; Schulte et al., 2012; Smit et al., 1996). It is tempting to ascribe the Tanis surges to tsunami waves traveling directly from the impact site in Yucatan up to North Dakota. However, even if the WIS were continuous at K-Pg time, it was estimated by DePalma et al. (2019) that the depositional window preceded the arrival time of any tsunami from the Gulf. The travel time of a tsunami from the impact site to Tanis would likely have been at least 18 hours and probably longer, depending upon the average depth of the WIS, which itself may not have constituted a continuous body of water in any case. This is clearly inconsistent with the temporal constraint based on interpretations of spherule arrival times, which constrain the deposits to within just several hours at most from the time of the impact. Thus some other mechanism for generating a 10 m water wave traveling up the Tanis River from the WIS must have been at play.

One candidate mechanism is direct water-wave excitation within the WIS due to seismic waves from the Chicxulub impact, which would have begun arriving at Tanis within only about 9 minutes after the impact. Such surge waves also have precedent in histor-

ical records, for example the Mw  $\sim 9$  earthquake in Japan in 2011 created seiches in Norwegian fjords with amplitudes of 1–2 m (Bondevik et al., 2013). The Chicxulub impact may have resulted in an earthquake with moment magnitude Mw  $\sim 11$  (Day & Maslin, 2005), leading DePalma et al. (2019) to suggest teleseismic seiches as a possible cause for the tsunami-like surge package. However, amplification by resonant seiching cannot be scaled up directly from earthquakes to impacts, as discussed further below, and seismic excitation of water waves in the WIS might have been more “impulsive” than resonant (as explained in detail below). Alternatively, strong ground motion might well have caused local sympathetic fault movement (Sleep & Olds, 2018; Smit et al., 1996), or underwater slope instability/collapse along the WIS shoreline. An entirely different class of excitation mechanisms would include water waves driven by atmospheric pressure waves associated with the expanding Chicxulub ejecta curtain (e.g., (Artemieva & Morgan, 2020)), which of course is the very source of the ejecta infall recorded in the surge deposits. Unfortunately, much less is known about the timing of such atmospheric disturbances (which would have had to precede the infall of large impact spherules) – indeed, even the temporal size distribution of ejecta/spherules remains only speculative.

In this paper we focus on models for direct seismic excitation of water waves within the WIS that may have propagated up the Tanis River, relying upon well-understood tsunami generation models. Yet even these models remain rather restricted, as the potential source time function for seismic radiation from the Chicxulub impact is highly variable, possibly ranging from highly-impulsive ( $\sim 50$ – $100$  seconds duration) due to the impact explosion itself, to many minutes if the rebound of the crater floor is strongly coupled seismically, as discussed further below. Another important caveat to note is the lack of concrete or verifiable data for certain key variables that form the basis for any mathematical modeling, including the dimensions of the Tanis River and WIS, due to an incomplete geologic record. These unknown variables include but are not limited to: the full paleogeographic extent of the WIS (including whether it extended to the paleo Gulf of Mexico in the terminal-Cretaceous or was a small, restricted, and landlocked basin); the slope of the terminal-Cretaceous WIS; the depth of the terminal-Cretaceous WIS; the fauna of the terminal-Cretaceous WIS; the position of the terminal-Cretaceous WIS paleoshoreline; the width of the Tanis River; the depth of the Tanis River; the funnel shape of the Tanis estuary; the arrival time of impact ejecta in the study area, which has a broad range of estimates based on contrasting prior research manuscripts. Of the aforementioned variables, none can be better-constrained through additional field efforts except for ejecta arrival time, largely because there is no terminal-Cretaceous geologic record of the WIS or any additional contemporaneous sections of the Tanis River. Therefore, to test the scenarios explored in this study required that assumptions be made for multiple variables concomitantly. Still there is much to be learned from simple models of seiche/tsunami excitation within the WIS, such as possible relations among seismic source duration and possible distances for material advection up the Tanis River from the WIS (constrained, e.g., by the intermixing of freshwater and marine fossils). So this study should be considered to be a starting point for unravelling the dynamics of the Tanis deposits, hopefully in time shedding more light on the details of the genesis of this remarkable record of the first moments of the Paleogene. Although no other comparable sites are presently known, surge event modeling might also suggest where such sites might be found, either within the Tanis/Hell Creek region itself, or at other sites along the WIS or elsewhere at K-Pg time.

## 2 Modeling of Water Wave Excitation in the WIS

DePalma et al. (2019) suggested that the tsunami-like surges forming the Tanis deposits could potentially be linked to seismic shaking generated by the impact, most likely created by seiching due to the seismic waves that reached the site within 10–15 minutes

following the impact. In this section we further explore the nature of a tsunami generated by teleseismic waves and some observations and implications.

Because different communities often interpret terms such as tsunami, surge, and seiche in different ways, we first summarize our use of this terminology in this paper. We use the term “surge” to refer to a distinct pulse of water that washed over the pointbar and left behind a deposit. The evidence at Tanis points to at least two distinct surges, which presumably resulted from a large disturbance propagating into the river from the body of water that it empties into. Such a disturbance (consisting perhaps of several waves) will be called the “tsunami” regardless of the manner in which it was generated, which is an open question that we hope to shed some light on in this paper. A “seiche” generally refers to a particular type of tsunami that presents as a periodic sloshing motion in an enclosed or semi-enclosed body of water such as a lake or harbor, and generally appears as a standing wave at the fundamental sloshing frequency determined by the topography. Observable wave motion is often excited by an external forcing (e.g. an earthquake) with significant energy at the sloshing frequency, and with sufficient duration that resonance causes growth of the standing wave with time.

With these definitions, we believe the use of the term “seiching” may be misleading in the context of the Tanis deposits. While teleseismic seiches have been observed at great distances in many historical earthquakes, they tend to be seen in bodies of water that are relatively narrow in the direction of maximum horizontal motion and that have fairly steep topography, which creates a larger response than gently sloping topography. In fact teleseismic seiching is often observed in swimming pools (which also have small dimensions and hence short sloshing periods, commensurate with high-frequency shaking) and in steep natural topography such as across fjords or deep rivers. A compilation of teleseismic seiching observed across the continental US following the 1964 Alaska earthquake by McGarr and Vorhis (1968) noted that the largest teleseismic seiches observed tended to be in reservoirs, and most others were cross-river seiches. In all cases at great distance from Alaska, the open-water amplitudes observed were a few cm at most.

Seiches with peak-to-trough amplitudes up to 1.5 m were observed in Norwegian fjords following the 2011 Tohoku Earthquake. Bondevik et al. (2013) found that they were most prevalent in portions of fjords oriented in the N-S direction, since the seismic waves from Japan came from the north. They showed through numerical simulations that the S-wave oscillating in the E-W direction was primarily responsible for the seiching observed in the narrow cross-fjord direction, and that the S-waves arriving in Norway had significant energy in the periods observed in the seiching (79–94 sec in most fjords). Moreover, the most significant waves were observed 5–10 minutes after the initial arrival of the S-waves, and increased further as the slower surface waves arrived, suggesting resonant amplification.

The seismic waves arriving at the Tanis site from the Chicxulub impact would have been considerably stronger than those arriving in Norway in 2011 or any tectonic earthquake in recorded history, and possibly with a different character than waves from a large earthquake. Much of the energy may have been in an initial jolt from the impact, followed by large-scale oscillations of the resulting molten rock at the impact site. Simulations such as those performed recently by Collins et al. (2020) and Range et al. (2022) suggest a period of 200–400 seconds for such oscillations.

Figure 2 shows the radial displacement, velocity, and acceleration of the long-period (40-500s) synthetic seismogram at a distance of 3100km from the impact site, indicating similar periods. This was computed using the normal mode summation theory (Gilbert, 1971; Woodhouse & Girnius, 1982) as implemented in the open-source code `modeslib` of Capdeville (2021). The eigenfrequencies and eigenfunctions were calculated for the reference earth model PREMQL6, which is a combination of the Preliminary Reference Earth Model (PREM) of Dziewonski and Anderson (1981) and the attenuation model

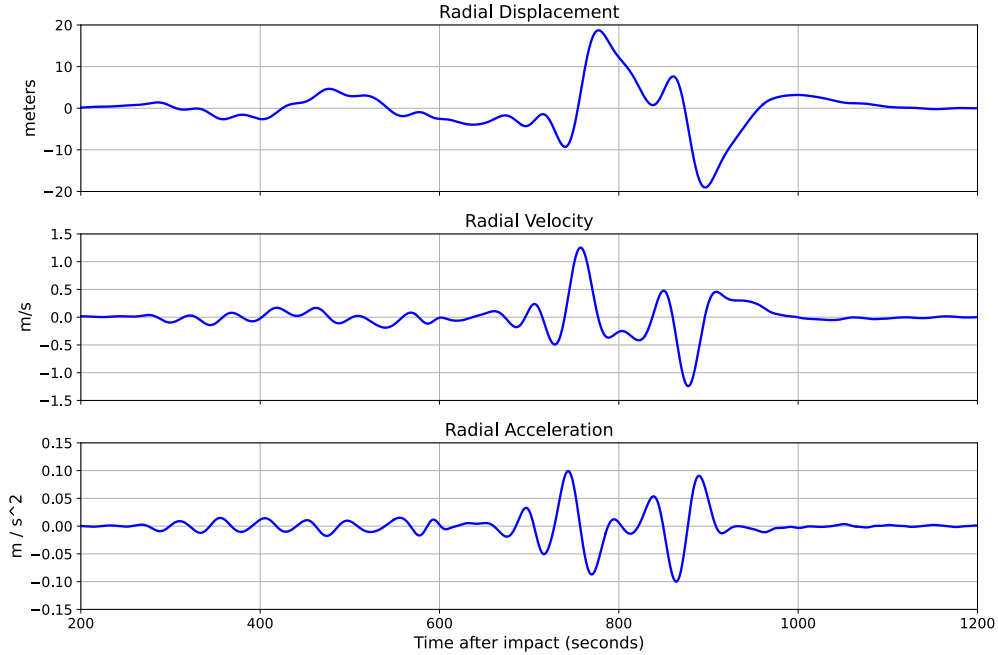


**Figure 2.** Radial displacement, velocity, and acceleration vs. time in seconds post-impact, at a site 3100 km distant. Computed using the normal mode summation theory, for a radial point source of moment magnitude 11.

QL6 of Durek and Ekström (1996). The maximum radial and angular orders considered were 100 and 1500, respectively, within a 1–200 mHz frequency range. A point source with a radial moment magnitude of 11, a half-duration of 60s, and a depth of 10km was utilized to generate the radial displacement synthetic seismogram. The half-duration and seismic moment are consistent with the assumptions of Meschede et al. (2011) and the cratering simulations of Collins et al. (2020) and Range et al. (2022), while the depth was based on the latter simulations. The excitation coefficients for each normal mode were calculated, and only the spheroidal modes were summed based on their respective excitation coefficients. A similar approach is discussed by Boslough et al. (1996) and by Meschede et al. (2011).

If the wave shown in Figure 2 were followed by a wave train of similar amplitude waves generated by the oscillations of the earth at the impact site, they could conceivably generate a classical seiche if the body of water was of suitable size, potentially generating a deposit consistent with the long-wavelength pulses at Tanis. Cross-river seiching is also a possibility. While the dimensions of the Tanis river are unknown and unconfirmable due to limitations of its preservation to a very small outcrop area, if the Tanis River were hypothetically 100 m wide and 10 m deep with nearly vertical sides, for example, then shallow water theory predicts the fundamental period would be approximately 200 s, as discussed further below. However, we believe a wave from cross-river seismic excitation might have an initial amplitude of only 2 m (based on equation (6) below), and considerable resonant amplification over several periods would be required to create the deposits observed. Such amplification could potentially have occurred and has not been ruled out at this time.

Sloshing from cross-river seiching, however, would not result in the distant transport of seawater and marine organisms to the Tanis site. The fact that marine fossils (including large  $\sim 10$  cm ammonite fragments) are intermixed with freshwater fish fossils

in the deposits suggests that the surges were generated in the WIS or an estuary environment and then traveled up the river to the Tanis site.

It is also possible that the initial seismic pulse seen in Figure 2, accompanied perhaps by a significant second wave due to ground oscillations at the impact site, is sufficient to generate the surges in a larger estuary and that these transported seawater up to the Tanis site, without the need for resonant amplification. Because there is a limit on how far seawater might have been transported upstream, we concur with DePalma et al. (2019) that the Tanis site must have been within a few km of the river mouth. This is explored in more detail in Section 3 below, but the upshot is that the amount of water transported upriver is bounded in terms of the amount of water displaced in the largest positive wave generated offshore. With the waves predicted from the direct seismic excitation that we have considered, relatively little water can be transported.

If the seismic waves did not directly produce surges of the sort observed in the deposits at Tanis, another possibility is that the teleseismic waves triggered a local event (such as the seafloor displacement during the Tohoku event) that in turn created the tsunami. One possibility is that a local earthquake was triggered that resulted in significant vertical displacement of the seafloor in the WIS, resulting in a long-period tsunami similar to those observed from megathrust events on subduction zones and consistent with the long-period surge deposit preserved at Tanis. Multiple faults, synclines, and anticlines related to the Laramide Orogeny and Cordilleran Orogenic Belt ran directly beneath the general geographic location of the WIS and were plentiful in the Williston Basin in which the study area resides. However, there is no geologic record of coeval marine deposits and we therefore lack geologic evidence for any such "megathrust" scale fault zones at K-Pg time in the vicinity of Tanis, precluding an assessment of the likelihood of this physically plausible scenario, which is not investigated in this study. It is noteworthy to mention that tsunamis generated by large subduction zone earthquakes have precedent in historical records and can bring seawater far inland, although still only a few km at most. For example, in 2011 the Sendai Plain in Japan was flooded as much as 6.8 km inland over dry land and waves propagated an additional 3–4 km upriver in the rivers crossing this plain (Adityawan et al., 2012; Nakajima & Koarai, 2011). In that event the coseismic displacement of the seafloor uplifted an area that extended about 100 km in the offshore direction. This created a wave with a spatial wavelength of this magnitude and hence a temporal period of order 30 minutes, consistent with videos and other evidence showing that the inland surge continued for 10s of minutes (Adityawan et al., 2012). Other discussions of inland transport of marine organisms are sparse in the literature, and generally also concern megathrust subduction zone events. For example, the tsunami generated by the 1945 Mw 8.5 Makran Subduction Zone earthquake was shown by Donato et al. (2008) to have transported bivalves 1–5 km into a shallow lagoon on the Arabian Sea. This was a major tsunami with runups up to 13 m and that again had wave periods from several 10s of minutes to an hour (Adams et al., 2018). By contrast, if the direct excitement of water by the Chicxulub impact had dominant periods on the order of a few minutes at most, then the resulting surge waves could not have advanced very far inland before the following trough reversed the flow.

Yet another possibility is that the teleseismic waves triggered a subaerial landslide or submarine mass failure that generated the tsunami. A mass failure over a sufficiently large portion of the seafloor could generate a significant tsunami with long-period waves, generating deposits consistent with what we see at Tanis. Mass failures of this nature have been documented on continental slopes, e.g. the Storegga slide off the coast of Norway 8100 years ago, with an estimated release volume of 2400–3200 km<sup>3</sup> and a runout distance of about 400 km. Tsunami deposits from this event have been documented in Scotland, England, and Denmark, e.g. by Bondevik et al. (1997); Fruergaard et al. (2015); Romundset and Bondevik (2011). Tsunami simulations of Kim et al. (2019) show tsunami heights of up to 15 m at some of these locations, exceeding that of Tanis. There is ev-

idence that many such submarine slides were triggered on continental slopes by the Chicxulub impact, as discussed for example by Day and Maslin (2005), Bralower et al. (1998), and Norris et al. (2000). Massive submarine slides are known to have occurred in the WIS in the Campanian and Maastrichtian (discussed further below) through normal processes without any known impact- or earthquake-related triggering event, so it would be surprising if seismic shaking from the Chicxulub impact did not cause equivalent or more pronounced widespread submarine sliding events throughout the WIS body of water. Regarding both the fault-offset and slope failure mechanisms (induced by the Chicxulub impact), consequent tsunamis within the WIS would likely have consisted of long-period waves (consistent with the fossil surge deposit) capable of propagation well up the Tanis River, along with advective transport of marine water some distance upstream. We do not, however, attempt to model such events in this paper, in no small part because we are unable to quantify massive coeval slope failure events near Tanis at K-Pg time due to lack of a geologic record for the coeval WIS.

### 3 Modeling the limits of upstream transport

The multi-pulse surge that formed the Tanis sediment package deposited both freshwater and seawater sediments and organisms at a maximum elevation of roughly 10 m above the river level. The majority of marine fossils at Tanis are microscopic, such as the marine dinoflagellates, or lightweight flakes of ammonite shell, and thus are maximally conducive for distant aqueous transport for as long as they are within transport capacity of the flow, indicating that their deposition would be compatible with the greater end of the spectrum for plausible up-river transport. We believe this was at most a few km, consistent with the local fossil record that includes brackish organisms indicative of close proximity to the paleoshoreline (DePalma et al., 2019). This is further justified in this section, where we present a simplified one-dimensional model of surge transport related to direct seismic excitation of water waves, using order of magnitude constraints on all the unknown aspects of this problem.

Note that a tsunami *wave* can propagate much longer distances upstream, and such waves have been observed in many historical events (Tolkova, 2018), but such a wave is generally not transporting (“advecting”) water very far, only energy. This is illustrated in Figure 3, which shows a cartoon of the propagation of a tsunami originating in the deeper water of the WIS or an estuary and then shoaling into shallow water and propagating up a river, as explained further below. The final frame, Figure 3(e), shows that eventually the wave is propagating in the freshwater of the river, and saltwater has been transported only from the river mouth to the dashed line that indicates the saltwater/freshwater interface.

The distance water is transported is determined by the horizontal velocity of the water as the wave passes by, together with the duration of the wave. The linearized shallow water equations often provide a good model for tsunami propagation (LeVeque et al., 2011), and in this case the wave shown in the cartoon would be propagating at speed  $\sqrt{gH}$  in water with an undisturbed depth  $H$  (where  $g = 9.81 \text{ m/s}^2$ ), while the depth-averaged horizontal component of the water velocity beneath a wave of amplitude  $\eta(x)$  (above the undisturbed surface) is given by

$$u = \eta(x)\sqrt{g/H}, \quad (1)$$

as shown in the SI. To compute how far water is transported in the deep water region, let  $A_1$  be the area under this hump,

$$A_1 = \int \eta(x) dx < L_1\eta_1^* \quad (2)$$

where we use  $L_1$  and  $\eta_1^*$  to denote the length of the hump and its maximum elevation, respectively. For a sinusoidal pulse as in Figure 3,  $A_1 = 0.5L_1\eta_1^*$ . It is also possible

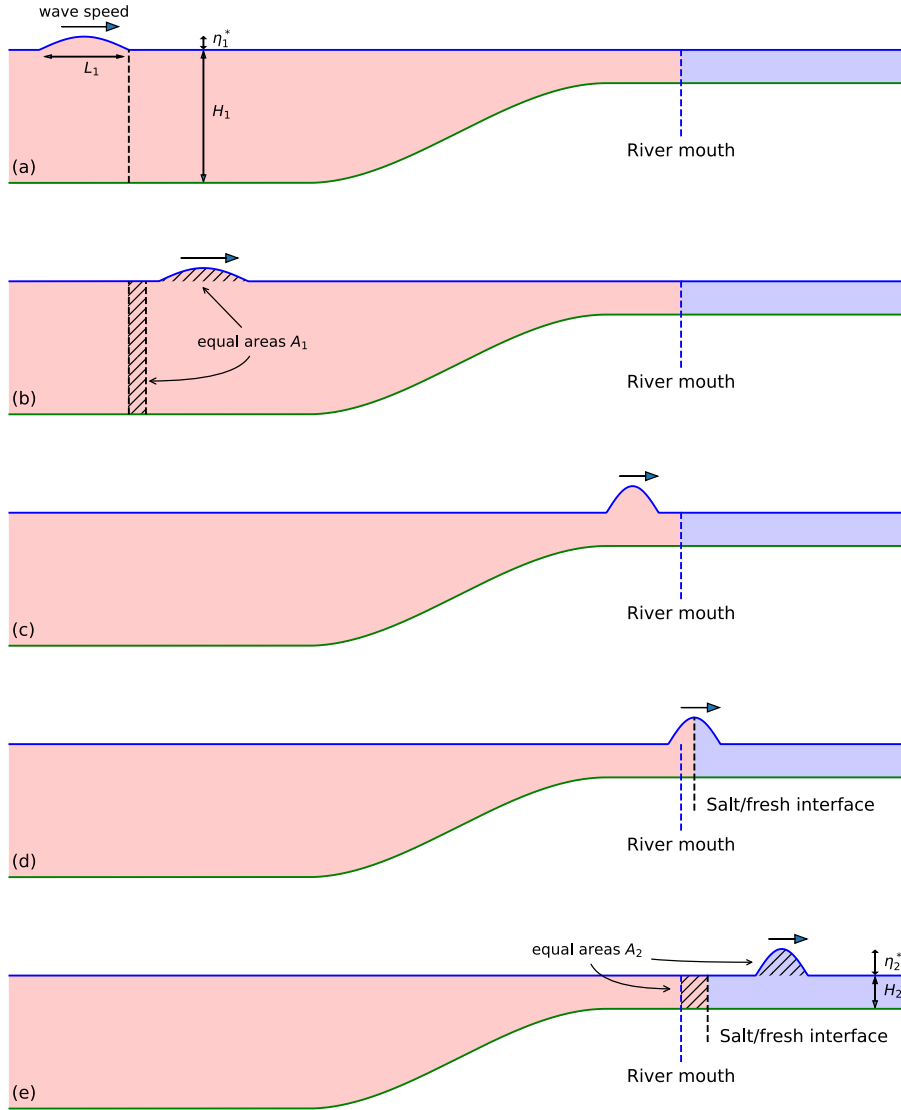


**Figure 3.** Cartoon (not to scale) showing the propagation of a tsunami as it shoals into shallow water and then propagates up a river. Figures (d) and (e) show the motion of the interface between saltwater (red) and freshwater (blue) as the wave passes by. In (e), the cross-hatched areas  $A_2$  are equal, and differ from  $A_1$  due to shoaling; see (4). See the text for discussion, and the Supplementary Information for more complete details.

to determine an upper bound on  $A_1$  directly from the peak horizontal ground displacement of the seismic forcing without knowing details of the source or topography, as discussed further below. The distance water is transported horizontally as the wave moves past is then approximately  $A_1/H_1$ , where  $H_1$  is the depth of the water in this region, as shown in the Supplementary Information (SI). By the time shown in Figure 3(b), the water at the dashed reference line shown in Figure 3(a) has moved to the right and the cross-hatched region shows the area traversed. By conservation of mass, this area must equal the area of the wave above the resting water depth, also shown by cross hatching in Figure 3(b). (Not drawn to scale; the displacement of the dashed reference line and the area traversed are exaggerated for clarity.)

As the wave moves into shallower water of depth  $H_2 < H_1$ , shoaling takes place, as illustrated in Figure 3(c). The amplitude of the wave typically increases while its length and speed decrease. The amplitude increase depends on the shape of the bathymetry (which is unknown for the terminal-Cretaceous WIS and hypothetically addressed here), but an upper bound is generally provided by the amplification factor  $C_G$  of Green’s Law (George et al., 2020),

$$\eta_2^* \leq C_G \eta_1^*, \quad \text{where } C_G = (H_1/H_2)^{1/4}. \quad (3)$$

This assumes the wave amplitude is still small relative to the water depth. As an example, if the waves moves from water of depth  $H_1 = 100$  m to  $H_2 = 10$  m, then  $C_G = 1.78$ . It is safe to assume that  $C_G < 2$  for the topography around the the WIS. Moreover, nonlinearity can lead to wave breaking and decay rather than amplification of the shoaling waves, as discussed further below.

The cartoon shown in Figure 3 is a one-dimensional vertical cross-section of a profile that is assumed to be constant in the direction into the page. In reality, there would likely be focusing as the estuary narrows to match the width of the river, a marked amplification that has been documented in modern historical tsunamis. In steep narrow valleys this focusing can be significant, but if the topography present in an estuary in the Tanis region had been shallow, this additional amplification might be at most another factor of 2.

Unlike the amplitude, the total mass of water transported by the wave *decreases* as the wave shoals, and moreover it is less sensitive to the shape of the topography, as shown by George et al. (2020). For the one-dimensional cartoon case, the area under the wave shown in Figure 3(c-e) has a value  $A_2 = r_s A_1$  where

$$r_s \equiv \frac{A_2}{A_1} = \frac{2}{1 + \sqrt{H_1/H_2}}. \quad (4)$$

This “shoaling ratio”  $r_s$  depends on the ratio of the deep water depth  $H_1$  to the river depth  $H_2$ , which are unfortunately not known for the terminal-Cretaceous WIS and are therefore treated here as hypothetical estimates. For example, if  $H_1/H_2 = 10$ , then  $r_s \approx 0.5$ , and  $r_s < 1$  for any ratio  $H_1/H_2 > 1$ .

By the final time shown in Figure 3(e), the tsunami is propagating entirely in the freshwater of the river, and again the cross-hatched areas are equal. The maximum upriver extent of saltwater can thus be calculated from the area under this propagating wave divided by the river depth,

$$x^* = A_2/H_2 = r_s A_1/H_2. \quad (5)$$

This formula assumes the tsunami amplitude in the river is less than the river depth  $H_2$ ; other considerations apply in the highly nonlinear case when this does not hold, but would not change the order of magnitude of upriver transport, and nonlinearity generally causes more rapid decay of the wave due to wave breaking.

The time shown in Figure 3(d) is perhaps of most interest for the Tanis site. At this time, the saltwater/freshwater interface is at the maximum of the hump, so that if

the wave exceeded the banks at this time (e.g. on a point bar when rounding a curve), then both freshwater and saltwater organisms might be deposited in this region. At earlier times the peak of the surge is purely saltwater while at later times it is purely freshwater. At this time the freshwater/saltwater interface is half of its final maximum value  $x^*$ , since half of the hump is composed of freshwater at this time. Tanis is unlikely to have been in exactly such a location, but must have been far enough downriver for saltwater to have reached it.

In order to apply (5) to our situation, we must estimate the area  $A_1$  or alternatively the length  $L_1$  and amplitude  $\eta_1^*$  arising from the seismic wave generated from the impact. The amplitude of a water wave generated by this motion depends greatly on the topography, and increases with both the water depth and the steepness of the bottom. With vertical walls and a flat bottom (with initial hypothetical water depth  $H_1$ ), an estimate of the maximum amplitude of the water surface displacement  $\eta$  can be derived from the linearized shallow water equations (see SI for details), as

$$\eta_1^* = \sqrt{H_1/g} U^*, \quad (6)$$

where  $g = 9.81 \text{ m/s}^2$  is the gravitational acceleration and  $U^*$  is the peak horizontal ground velocity. Under these same conditions, the spatial length of a wave generated by a pulse of duration  $T$  seconds is roughly  $L_1 = \sqrt{gH_1} T$  meters. In this case  $A_1 \leq L_1 \eta_1^* = H_1 U^* T$ . Another way to derive this is to note that the wall moves distance at most  $U^* T$  and hence displaces an area of water bounded by this distance times the depth  $H_1$  of the water adjacent to the wall. This argument extends to give a bound on  $A_1$  that is independent of both the topography, assuming it slopes down to some maximum depth  $H_1$ , and the details of the seismic source. If  $R^*$  denotes the peak horizontal ground displacement in the seismic forcing (with  $R^* \leq U^* T$ ), then the corresponding pulse of water has area bounded by  $A_1 \leq H_1 R^*$ , as shown in the SI.

Using this bound in (5) gives

$$x^* < r_s R^* H_1 / H_2. \quad (7)$$

Consider the ground motion shown in Figure 2, for example, with peak displacement of approximately 10 m (assuming the river mouth is oriented so that the negative displacement peak gives the maximum positive wave aimed at the river). We also observe a peak velocity of roughly 1.2 m/s and a peak acceleration of 0.1  $\text{m/s}^2$ . The actual dimensions of the WIS at that time are unknown, but as a gross upper bound, assume the WIS has a depth of  $H_1 = 200$  m and is bounded by a vertical wall, in a river of depth  $H_2 = 10$  m. Using  $R^* = 10$ ,  $H_1/H_2 = 20$ , and  $r_s = 0.5$  in (7) gives  $x^* < 200$  m as an estimate of the maximum distance of salt water intrusion. Using a peak velocity  $U^* = 1.2 \text{ m/s}$ , (6) gives a wave height  $\eta_1^* \approx 5.4$  m.

Although these values were estimated using the linearized shallow water equations, a numerical simulation using the full nonlinear shallow water equations with this geometry, shown in Figure 4(a), confirms that these values are roughly the right order of magnitude. Details of the numerical modeling are given in the SI. One notable difference in the simulation is that the wave amplitude barely increases during shoaling because the nonlinearity leads to shock formation (wave breaking) that reduces the amplitude of the peak. This continues as the wave moves into and up the river so that the 7 m wave amplitude seen at 1140 seconds decays to only 5 m by time 1230s. The final time shows the maximum saltwater intrusion, which is somewhat larger than estimated, but still less than 400 m.

The simulation in Figure 4(b) shows the same wave approaching a shallower river with depth 1 m. In this case the estimate for  $x^*$  would increase by a factor of 10 to 2000 m. At time 1230 seconds the saltwater/freshwater interface is at 969 m and still moving to the right, and in this case the wave amplitude has again decreased to about 5 m.

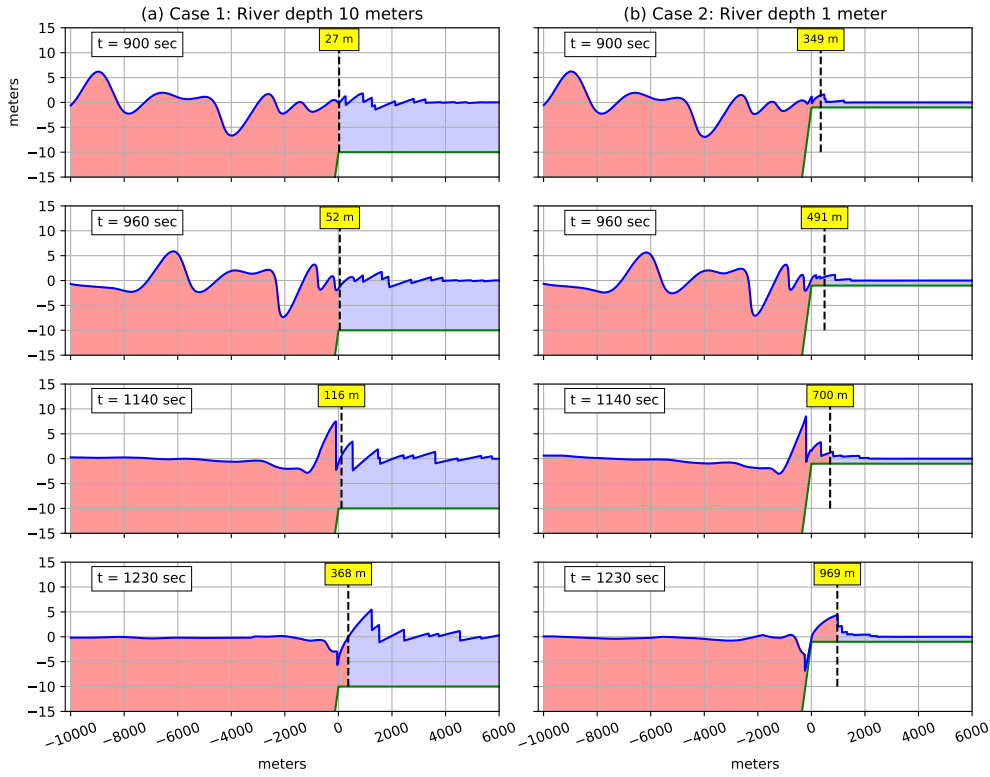


**Figure 4.** Numerical simulations (using nonlinear shallow water equations) of the tsunami generated by the seismic signal shown in Figure 2 in a basin of depth 200 m bounded by a wall on the left and a “river” on the right. The vertical dashed line shows the interface between salt-water to the left and freshwater to the right, and the distance from the river mouth at  $x = 0$  to this interface is noted in the attached box. (a) The left column is for a river depth of 10 m. (b) The right column is for a river depth of 1 m. The plots show only the upper 15 m of the basin, which extends to a depth of 200 m from the vertical wall boundary at  $x = -10000$  m to  $x = -5000$  m and then slopes up linearly to the river depth at  $x = 0$ . This gently sloping topography maximizes shoaling.

The waves shown here decrease dramatically in amplitude if a more reasonable basin topography is used instead of a vertical wall of height 200 m at the left boundary. A gently sloping seafloor would create waves with no greater area  $A_1$  than the wall case considered here. They may be more spatially spread out, however, leading to smaller amplitude waves, and more potential cancellation of positive and negative waves. This is discussed more in the SI with some additional simulations.

Rather than wave generation in a deep basin, a more likely scenario is that the surge waves were generated by steeper local relief in the vicinity of the mouth of the river, perhaps in a small bay with steeper sides but much smaller depth than 200 m, giving a correspondingly smaller value of  $x^*$ . The steep topography of the incised river valley at Tanis argues against a very shallow topography and instead suggests an intermediate topographical condition near the river. However, even with steep sides a smaller depth gives rise to correspondingly smaller waves. For example, if  $H_1 = 20$  m in the calculations above, then the estimated transport distances would decrease by a factor of 10, to  $x^* < 20$  m or 200 m for river depths of 10 or 1 m, respectively. Amplification due to focusing near a river mouth could increase all of these values to some extent, but the general conclusion is that saltwater transport via this mechanism would be consistent with constraints for modern tsunami waves traveling upriver.

In the SI we provide more details of these calculations. Many simplifying assumptions are made in doing this, not only that the situation is purely one-dimensional, but also that the initial saltwater/freshwater interface is a sharp interface at the river mouth, which might not be true in a brackish estuary environment. We also assume this interface remains sharp, while in practice there would certainly be turbulent mixing as the wave goes by. The estimates are based on the linearized one-dimensional shallow water equations, which do not model the full dynamics. However, the main impact of adding nonlinearity, as noted in the simulations of Figure 4, would be to potentially introduce wave breaking in the surge as it moved into shallower water, which would further reduce the wave height and inland transport distance relative to what has been estimated here.

We also ignore the elevation gain of the river bed moving upriver and the flow of the river, along with frictional drag forces, which could have a significant effect in a shallow river. All of these would further reduce the maximum upstream extent of saltwater. Finally, we note that the distance marine sediment (and the marine fossils found at the Tanis site) would be transported upstream might be even less than the distance the seawater intrudes, as observed on the Sendai Plain in Japan in 2011 where the inland limit of sediment deposition was 57–76 percent of the seawater inundation distance along post-tsunami transects (Abe et al., 2012).

#### 4 Other Potential Surge Excitation Mechanisms

The foregoing sections have explored the direct excitation of water waves at Tanis by seismic waves, which would have begun arriving at Tanis about 9 minutes after the Chicxulub impact. This might have occurred either by direct water wave excitation from the initial seismic pulse within the nearby WIS, or, as originally hypothesized, via seiche-like resonant waves. The temporal context considered here presents some challenges for both mechanisms in terms of the necessary 10 m amplitude and sustained upriver transport of marine water, with the classical seiche-like mechanism requiring many tens of minutes to develop for resonant amplification (which has not yet been completely ruled out based on geologic evidence). Both mechanisms would be more feasible if the effective source process time for seismic radiation from Chicxulub is considerably longer than what we have considered so far (as shown in Figure 2).

Alternative mechanisms not examined by this study also invoke excitation by the arrival of large-amplitude seismic waves, namely sympathetic fault displacement beneath

the WIS, and seismic triggering of large slope failure events within or into the WIS. Vertical offset along a large fault or faults beneath the WIS could cause long-period water wave excitation, which would be helpful in explaining the Tanis surges and more consistent with the deposit. The  $M_w \sim 11$  Chicxulub impact would likely have triggered earthquakes worldwide, and several authors have suggested that large fault movements in the Western US may have been caused by the Chicxulub-generated seismicity. Sleep and Olds (2018) described evidence for large normal-fault displacements terminating at the K-Pg boundary at outcrops within Madrid and Long’s Canyon in Colorado (well south of Tanis). While the recorded offsets were not within the WIS, nor were they likely large enough to have generated a local tsunami compatible with the Tanis surges, they demonstrate that impact-triggered fault displacement was occurring in the Western Interior. Additionally, while major faults possibly existed in the WIS at the KPg boundary, it is impossible to quantify them because all coeval WIS strata have been erased by erosion and no longer exist. Even so, it is none the less important to note that the Williston Basin, within which Tanis is located, is known to have been tectonically active, including multiple fault and anticline systems associated with the Laramide orogeny and Cordilleran Orogenic Belt. It is also worthwhile to note that fault displacement of sufficient magnitude also need not have been restricted to close proximity to the study area, it could have occurred elsewhere in the geographically expansive WIS provided it was close enough for the surge waves to arrive in the expected time interval.

Another possible seismically-induced mechanism, not dependent on existing faults, is that of land sliding into, or slope collapse within, the WIS. The Chicxulub impact induced large-scale slope collapse events in the circum-Atlantic region (Day & Maslin, 2005), such that wet sediment slope failure along the margins of the WIS at K-Pg time might be expected as well. Further highlighting this likelihood, submarine landslides, slope collapse, and mass-wasting prior to impact were numerous in the WIS, some of which were sufficiently massive to create large-scale sediment mobilization resulting in contorted, turbulent beds greater than 5 meters thick over broad areas up to several hundred square km (Landman et al., 2013). These submarine landslides could have extended over large areas, potentially resulting in long-period waves. We consider submarine mass failures a plausible mechanism that are certainly worthy of more investigation.

Another class of mechanisms are those due to the propagation of waves and ejecta through the atmosphere and through space. However, atmospheric waves in the far-field from Chicxulub would have propagated at slightly subsonic speeds ( $\sim 300$  m/sec or less), and thus could not have arrived at Tanis in time to explain the simultaneous infall of ejecta (spherules). Such mechanisms would include both the atmospheric blast wave itself, as well as potential Lamb waves such as highlighted from the recent 2022 Hunga Tonga Hunga Ha’apai eruption, as simulated by Kubota et al. (2022), for example. However, another potential mechanism is that of the atmospheric pressure and heat wave associated with the expansion of the very ejecta curtain responsible for the impact spherules themselves. Recent simulations confirm that the ejecta would have traveled around the Earth’s uppermost atmosphere, and in space, at speeds far exceeding the low-altitude sound speed (Artemieva & Morgan, 2020), as hypothesized by Alvarez (1996). Indeed, that is why the impact spherules arrive at Tanis so quickly. (We note that spherules must also settle through the atmosphere, likely on a timescale of about an hour — an effect neglected by Alvarez (1996)). Thus their arrival time is likely of order 1.5–2 hours or so post-impact.) This mechanism surely deserves further exploration, although recent simulations of the expanding ejecta curtain suggest that induced winds in the lower atmosphere were likely not in excess of several tens of meters/second, and therefore not likely capable of generating the large water waves necessary to explain the  $\sim 10$  meter surges observed at Tanis (Joanna Morgan, personal communication).

## 5 Future Fieldwork and Observations

The Tanis site was only recently described as a complex ejecta-bearing multi-pulse surge deposit (DePalma et al., 2019), and the overriding interest so far has been in the spectacular paleontological finds there that comprise a snapshot of the first moments of the Paleogene. The foregoing sections suggest the benefit of the ongoing work being undertaken, including deeper understanding of the nature of these deposits, their implications for the global (far-field) aftermath of the Chicxulub impact, and additional detailed information on their emplacement. In particular, although we are certain that these surges occurred within the first  $\sim 2$  hours after the impact, additional detailed information on their duration and on the time interval that separates them could shed more light on the potential excitation mechanisms.

The proximity of the Tanis site to the shoreline of the WIS at K-Pg time also remains a matter of speculation, informed in part by the anecdotal short upstream transport of marine fossils suggested by historical tsunamis and the simplified modeling presented above for a seismic surge of the sort that might have been directly triggered by the Chicxulub impact. Similarly, an obvious question is whether or not other Tanis-like deposits may lie either undiscovered at the surface, or concealed beneath overlying post-K-Pg deposits, remaining a tantalizing possibility for expanding our understanding of what happened at Tanis in a more regional context.

As mentioned earlier in this paper, of the many variables that are unknown yet critical to fully reconstructing the surge event, only the arrival time of ejecta, and possibly the timing and duration of the surge pulses, could be further refined by additional field work, the rest remaining unknown and unverifiable due to their absence from the geologic record. Even so, additional work in the field could potentially better resolve the timing of the surge pulses and/or better constrain the arrival time for ejecta. More examination of the stratigraphic and sedimentological data already collected (DePalma et al., 2019), possibly augmented by additional sedimentology of the surge deposits themselves, and additional quantitative grain-size analysis, could potentially yield important information on water current speeds through the section, and hence the timescale for their deposition (Huntington et al., 2007). Likewise, further examination of the data could hopefully shed light upon the time interval separating the two surges, which would provide an important constraint in discriminating among possible seiche-like mechanisms. Similarly, it could be informative to gain additional insight into the underlying point bar sand deposits.

The region surrounding Tanis might, in time, also reveal other similar sites, although so far efforts to this end have not been successful. It is also possible that remote sensing or field geophysical methods might reveal areal extensions of the Tanis deposits, and efforts to that end are being explored.

In summary, we hope that our quantitative exploration of seismically-induced water waves at Tanis may lead to additional field observations and numerical experiments, which could shed additional light on the way(s) in which the Chicxulub impact event directly or indirectly played a role in triggering the surge event at Tanis.

## 6 Conclusions

The discovery of a multi-pulse  $\sim 10$  m surge event deposit at exactly K-Pg time at Tanis, North Dakota represents an extraordinary opportunity to understand far-field events caused by the Chicxulub impact, and their relation to the K-Pg mass extinction. The timing of these surges relative to the in-fall of impact-generated spherules suggests seismic excitation by the Mw 11 Chicxulub-induced earthquake within the Western Interior Seaway (WIS) as a plausible mechanism, including direct excitation of water waves by seismic ground motion, or indirectly via regional slope failure or fault slip events. In

this study, we explored one of these (direct seismic excitation of water within the WIS) that might have generated the surge pulses that propagated up the Tanis river to the point bar where the surges were recorded geologically. Synthetic seismograms for the Chicxulub-induced earthquake with the hypothetical parameters explored here suggest that very large (meters in amplitude) water waves could have been induced in the WIS via direct excitation of water. However, the relatively short-period nature of these modeled waves are inconsistent with the long-period tsunami-like pulses that emplaced the Tanis deposit, and, along with attenuation during upriver flow, decrease the likelihood of this mechanism. If the effective source process time associated with the Chicxulub earthquake were 10s of minutes, as opposed to the few minutes modeled in the synthetic seismogram, then greater upriver transport of WIS marine water is more plausible, as in large subduction zone earthquakes. This suggests that more attention is needed to the generation of long-period seismic waves at the impact site, perhaps due to crater collapse/relaxation mechanisms. More generally, the magnitude of the seismic wave generated by the Chicxulub impact is poorly constrained, and it would be particularly valuable to obtain seismic waveforms directly from full multiphysics simulations of impacts, such as those performed by Collins et al. (2020) and Range et al. (2022). We have shown simplified one-dimensional simulation results for one plausible seismic mechanism to illustrate some of the issues involved, but we do not view the modeled amplitudes as conclusive.

Other seismically-related mechanisms discussed include slope failure, for which there is much evidence in the WIS during the late Cretaceous; and sympathetic slip of large tectonic faults, for which there is evidence for Laramide-related faults and potentially others elsewhere in the geographically expansive WIS, but we have not explored these mechanisms in this paper. Large water waves might also have been generated by the atmospheric effects of the in-fall of Chicxulub ejecta traveling through space on ballistic trajectories at supersonic speeds to the Tanis site, but preliminary estimates of the strength of such water waves suggests that the amplitudes would likely have been less pronounced than the  $\sim 10$  m amplitudes of the two Tanis surge pulses. Therefore, more theoretical modeling work can aid on several fronts. There may be added benefit for additional field work on the nature of the surge deposits to further define the duration and time-separation of the water surges, which could refine the initial modeling work on seismically-induced water waves emanating from the WIS, as described in this paper. Thus, although we can place important tentative constraints on the possible triggering event, we believe that a wealth of important information about the K-Pg impact and mass extinction event remains to be elucidated by further study of the Tanis surge deposits as well as the further study of possible mechanisms for their deposition.

## 7 Open Research

No new datasets were used in this research. The synthetic seismograms shown in Figure 2 were computed using the the open-source code `modeslib` of Capdeville (2021). The tsunami simulations shown in Figure 4 and in the SI were computed using the open source GeoClaw software (Clawpack Development Team, 2023). The input code for both of these models is archived on Zenodo (LeVeque, 2024) and is also available at

<https://github.com/rjleveque/ChicxulubTanisSurge>.

## Acknowledgments

We benefited from numerous discussions with other experts over the course of this project, including Nataila Artemeva, Joanna Morgan, Barbara Romanowicz, and Brian Toon. Anonymous referees also provided valuable feedback that led to substantial revisions. Responsibility for the modeling assumptions ultimately made, and the conclusions reached, lie solely with the authors.

## References

- Abe, T., Goto, K., & Sugawara, D. (2012). Relationship between the maximum extent of tsunami sand and the inundation limit of the 2011 Tohoku-oki tsunami on the Sendai Plain, Japan. *Sedimentary geology*, *282*, 142-150.
- Adams, L. M., Atwater, B. F., & Hasan, H. (2018). Karachi tides during the 1945 Makran tsunami. *Geosci. Lett.*, *5*, 1–13. doi: 10.1186/s40562-018-0121-z
- Adityawan, M. B., Roh, M., Tanaka, H., Mano, A., & Udo, K. (2012). Investigation of tsunami propagation characteristics in river and on land induced by the Great East Japan earthquake 2011. *Journal of Earthquake and Tsunami*, *06*, 1250033. doi: 10.1142/S1793431112500339
- Alvarez, W. (1996). *Trajectories of ballistic ejecta from the chicxulub crater*. Special Paper 307, Geological Society of America.
- Artemieva, N., & Morgan, J. (2020). Global K-Pg Layer Deposited From a Dust Cloud. *Geophys. Res. Lett.*, *47*(6), e2019GL086562. doi: 10.1029/2019GL086562
- Bondevik, S., Gjevik, B., & Sørensen, M. B. (2013). Norwegian seiches from the giant 2011 Tohoku earthquake. *Geophysical Research Letters*, *40*, 3374–3378. doi: <https://doi.org/10.1002/grl.50639>
- Bondevik, S., Svendsen, J. I., & Mangerud, J. (1997). Tsunami sedimentary facies deposited by the Storegga tsunami in shallow marine basins and coastal lakes, western Norway. *Sedimentology*, *44*, 1115–1131. doi: 10.1046/j.1365-3091.1997.d01-63.x
- Boslough, M. B., Chael, E. P., Trucano, T. G., Crawford, D. A., & Campbell, D. L. (1996). Axial focusing of impact energy in the Earth's interior: A possible link to flood basalts and hotspots. In G. Ryder, D. E. Fastovsky, & S. Gartner (Eds.), *The Cretaceous-Tertiary Event and Other Catastrophes in Earth History* (Vol. 307). Geological Society of America. doi: 10.1130/0-8137-2307-8.541
- Bourgeois, J., Hansen, T. A., Wiberg, P. L., & Kauffman, E. G. (1988). A Tsunami Deposit at the Cretaceous-Tertiary Boundary in Texas. *Science*, *241*(4865), 567–570. doi: 10.1126/science.241.4865.567
- Bralower, T. J., Paull, C. K., & Mark Leckie, R. (1998). The Cretaceous-Tertiary boundary cocktail: Chicxulub impact triggers margin collapse and extensive sediment gravity flows. *Geology*, *26*(4), 331–334. doi: 10.1130/0091-7613(1998)026<0331:TCTBCC>2.3.CO;2
- Capdeville, Y. (2021). *modeslib software*. <https://gitlab.univ-nantes.fr/capdeville-y/modeslib>.
- Clawpack Development Team. (2023). *Clawpack software*. <http://www.clawpack.org>. doi: 10.17605/osf.io/kmw6h
- Collins, G. S., Patel, N., Davison, T. M., Rae, A. S. P., Morgan, J. V., & Gulick, S. P. S. (2020). A steeply-inclined trajectory for the Chicxulub impact. *Nature Communications*, *11*, 1480. doi: 10.1038/s41467-020-15269-x
- Day, S., & Maslin, M. (2005). Linking large impacts, gas hydrates, and carbon isotope excursions through widespread sediment liquefaction and continental slope failure: The example of the K-T boundary event. In *Special Paper of the Geological Society of America* (Vol. 384, pp. 239–258). doi: 10.1130/0-8137-2384-1.239
- DePalma, R. A., Oleinik, A. A., Gurche, L. P., Burnham, D. A., Klingler, J. J., McKinney, C. J., . . . Manning, P. L. (2021). Seasonal calibration of the end-cretaceous Chicxulub impact event. *Sci Rep*, *11*(1), 23704. doi: 10.1038/s41598-021-03232-9
- DePalma, R. A., Smit, J., Burnham, D. A., Kuiper, K., Manning, P. L., Oleinik, A., . . . Alvarez, W. (2019). A seismically induced onshore surge deposit at the KPg boundary, North Dakota. *PNAS*, *116*(17), 8190–8199. doi: 10.1073/pnas.1817407116

- Donato, S. V., Reinhardt, E. G., Boyce, J. I., Rothaus, R., & Vosmer, T. (2008). Identifying tsunami deposits using bivalve shell taphonomy. *Geology (Boulder)*, *36*(3), 199-202.
- Durek, J. J., & Ekström, G. (1996). A radial model of anelasticity consistent with long-period surface-wave attenuation. *Bull. Seis. Soc. Amer.*, *86*, 144-158. doi: 10.1785/BSSA08601A0144
- Dziewonski, A. M., & Anderson, D. L. (1981). Preliminary reference earth model. *Physics of the Earth and Planetary Interiors*, *25*, 297-356. doi: 10.1016/0031-9201(81)90046-7
- Engel, M., Pilarczyk, J., May, S. M., Brill, D., & Garrett, D. E. (2020). *Geological records of tsunamis and other extreme waves*. San Diego: Elsevier Science.
- Fruergaard, M., Piasecki, S., Johannessen, P., Noe-Nygaard, N., Andersen, T., Pejrup, M., & Nielsen, L. (2015). Tsunami propagation over a wide, shallow continental shelf caused by the Storegga slide, southeastern North Sea, Denmark. *Geology*, *43*(12), 1047–1050. doi: 10.1130/G37151.1
- George, J., Ketcheson, D. I., & LeVeque, R. J. (2020). Shoaling on Steep Continental Slopes: Relating Transmission and Reflection Coefficients to Green’s Law. *Pure Appl. Geophys.*, *177*(3), 1659–1674. doi: 10.1007/s00024-019-02316-y
- Gilbert, F. (1971). Excitation of the normal modes of the earth by earthquake sources. *Geophys. J. Int.*, *22*, 223-226. doi: <https://doi.org/10.1111/j.1365-246X.1971.tb03593.x>
- Huntington, K., Bourgeois, J., Gelfenbaum, G., Lynett, P., Jaffe, B., Yeh, H., & Weiss, R. (2007). Sandy signs of a tsunami’s onshore depth and speed. *EOS*, *88*, 577–578. Retrieved from [http://www.agu.org/journals/eo/eo0752/2007E052\\_tabloid.pdf](http://www.agu.org/journals/eo/eo0752/2007E052_tabloid.pdf)
- Kim, J., Løvholt, F., Issler, D., & Forsberg, C. F. (2019). Landslide Material Control on Tsunami Genesis—The Storegga Slide and Tsunami (8,100 Years BP). *Journal of Geophysical Research: Oceans*, *124*, 3607–3627. doi: 10.1029/2018JC014893
- Kubota, T., Saito, T., & Nishida, K. (2022). Global fast-traveling tsunamis driven by atmospheric Lamb waves on the 2022 Tonga eruption. *Science*, *377*, 91–94. doi: 10.1126/science.abo4364
- Landman, N. H., Remin, Z., Garb, M. P., & Chamberlain, J. A. (2013). Cephalopods from the Badlands National Park area, South Dakota: Re-assessment of the position of the Cretaceous/Paleogene boundary. *Cretaceous Research*, *42*, 1–27. doi: 10.1016/j.cretres.2012.12.011
- LeVeque, R. J. (2024). *rjleveque/ChicxulubTanisSurge: February 1, 2024 (submitted\_revised-1)*. [Software] Zenodo. doi: 10.5281/zenodo.10606185
- LeVeque, R. J., George, D. L., & Berger, M. J. (2011). Tsunami modelling with adaptively refined finite volume methods. *Acta Numerica*, *20*, 211 – 289. doi: 10.1017/S0962492911000043
- McGarr, A., & Vorhis, R. C. (1968). *Seismic Seiches from the March 1964 Alaska Earthquake* (Tech. Rep. No. PP 544-E). USGS Professional Paper. Retrieved from <https://pubs.usgs.gov/pp/0544e/>
- Meschede, M. A., Myhrvold, C. L., & Tromp, J. (2011). Antipodal focusing of seismic waves due to large meteorite impacts on Earth. *Geophysical Journal International*, *187*, 529–537. doi: 10.1111/j.1365-246X.2011.05170.x
- Nakajima, H., & Koarai, M. (2011). Assessment of tsunami flood situation from the Great East Japan Earthquake. *Bulletin of the Geospatial Information Authority of Japan*, *59*.
- Norris, R. D., Firth, J., Blusztajn, J. S., & Ravizza, G. (2000). Mass failure of the North Atlantic margin triggered by the Cretaceous-Paleogene bolide impact. *Geology*, *28*, 1119–1122. doi: 10.1130/0091-7613(2000)28(1119:MFOTNA)2.0.CO;2
- Range, M. M., Arbic, B. K., Johnson, B. C., Moore, T. C., Titov, V., Adcroft, A. J.,

- ... Wang, H. (2022). The Chicxulub impact produced a powerful global tsunami. *AGU Advances*, 3, e2021AV000627. doi: 10.1029/2021AV000627
- Romundset, A., & Bondevik, S. (2011). Propagation of the Storegga tsunami into ice-free lakes along the southern shores of the Barents Sea. *Journal of Quaternary Science*, 26, 457–462. doi: 10.1002/jqs.1511
- Schulte, P., Smit, J., Deutsch, A., Salge, T., Friese, A., & Beichel, K. (2012). Tsunami backwash deposits with Chicxulub impact ejecta and dinosaur remains from the Cretaceous–Palaeogene boundary in the La Popa Basin, Mexico. *Sedimentology*, 59, 737–765. doi: 10.1111/j.1365-3091.2011.01274.x
- Sleep, N. H., & Olds, E. P. (2018). Remote Faulting Triggered by Strong Seismic Waves from the Cretaceous–Paleogene Asteroid Impact. *Seismological Research Letters*, 89(2A), 570–576. doi: 10.1785/0220170223
- Smit, J., Roep, T. B., Alvarez, W., Montanari, A., Claeys, P., Grajales-Nishimura, J. M., & Bermudez, J. (1996). Coarse-grained, clastic sandstone complex at the K/T boundary around the Gulf of Mexico: Deposition by tsunami waves induced by the Chicxulub impact? In G. Ryder, D. E. Fastovsky, & S. Gartner (Eds.), *The Cretaceous-Tertiary Event and Other Catastrophes in Earth History* (Vol. 307). Geological Society of America. doi: 10.1130/0-8137-2307-8.151
- Tolkova, E. (2018). *Tsunami Propagation in Tidal Rivers*. Cham: Springer International Publishing. doi: 10.1007/978-3-319-73287-9
- Woodhouse, J. H., & Girnius, T. P. (1982). Surface waves and free oscillations in a regionalized earth model. *Geophys. J. Int.*, 68, 653–673. doi: 10.1111/j.1365-246X.1982.tb04921.x

# Supporting Information for “Plausible Mechanisms for Tsunami-like Surge Deposits Due to the Chicxulub Impact...”

Randall J. LeVeque<sup>1</sup>, Robert A. DePalma<sup>2</sup>, Carrie Garrison-Laney<sup>3</sup>, Satish

Maurya<sup>4</sup>, Jan Smit<sup>5</sup>, Mark A. Richards<sup>6</sup>

<sup>1</sup>Department of Applied Mathematics, University of Washington, Seattle, USA

<sup>2</sup>Department of Natural History, University of Manchester, UK

<sup>3</sup>Washington Sea Grant, University of Washington, Seattle, USA

<sup>4</sup>Department of Earth Sciences, IIT Bombay, Mumbai, Maharashtra, India

<sup>5</sup>Faculty of Earth and Life Sciences, Institute of Earth Sciences, Vrije Universiteit Amsterdam, Netherlands.

<sup>6</sup>Department of Earth and Space Sciences, University of Washington, Seattle, USA

## Contents of this file

1. Text S1. Shallow water equations.
2. Text S2. Numerical simulations.
3. Captions for Movies S1 to S4
4. Text S3. GeoClaw software.
5. Figures S1 to S3

---

Corresponding author: R. J. LeVeque, Department of Applied Mathematics, University of Washington, Seattle, WA 98195-3925, USA. (rjl@uw.edu)

**Additional Supporting Information (Files uploaded separately)**

1. Movies S1 to S4

**Introduction**

We include some details of the standard nonlinear and linearized shallow water equations and the derivation of the wave speed and amplitude that appear in Section 3 of the paper.

We also present additional numerical simulations using the one-dimensional nonlinear shallow water equations for the simple geometry of a basin connected to a river, showing two more cases to supplement Figure 4 of the paper. The simulation code is briefly described, which uses the open source GeoClaw software.

**Text S1. The shallow water equations**

The nonlinear shallow water equations in one space dimension are

$$\begin{aligned} h_t + (hu)_x &= 0 \\ (hu)_t + \left( hu^2 + \frac{1}{2}gh^2 \right)_x &= -ghB_x \end{aligned} \tag{1}$$

where  $h(x, t)$  is the water depth,  $u(x, t)$  is the depth-averaged horizontal velocity,  $hu$  the momentum,  $g = 9.81$  the gravitational acceleration. On the right hand side of the momentum equation,  $B(x)$  represents the topography/bathymetry with the convention that  $B(x) > 0$  corresponds to onshore (initially dry) land and  $B(x) < 0$  offshore. LeVeque, George, and Berger (2011) discuss these equations and their application to tsunami modeling, and provide a more detailed discussion of the linearization and eigenstructure used below.

If we linearize about a flat surface and zero velocity, then the equations can be written as

$$\begin{aligned} \eta_t + (H(x)u)_x &= 0 \\ u_t + g\eta_x &= 0 \end{aligned} \tag{2}$$

where  $\eta(x, t)$  is the surface elevation ( $\eta = 0$  for undisturbed water,  $\eta(x, t) = B(x) + h(x, t)$  in the nonlinear equations),  $H(x) = \min(-B(x), 0)$  is the undisturbed water depth,  $u(x, t)$  is the depth-averaged horizontal velocity, and  $g$  is the gravitational constant.

Equation (2) is a linear hyperbolic system of the form  $q_t + (Aq)_x = 0$ , with coefficient matrix

$$A = \begin{bmatrix} 0 & H \\ g & 0 \end{bmatrix}. \quad (3)$$

The eigenvalues of this matrix are  $\lambda = \pm\sqrt{gH}$ , indicating that in one dimension waves can propagate in either direction at the gravity wave speed  $\sqrt{gH}$ .

The eigenvectors are

$$\begin{aligned} r^1 &= \begin{bmatrix} 1 \\ -\sqrt{g/H} \end{bmatrix}, & \text{for } \lambda^1 &= -\sqrt{gH}, \\ r^2 &= \begin{bmatrix} 1 \\ +\sqrt{g/H} \end{bmatrix}, & \text{for } \lambda^2 &= +\sqrt{gH}. \end{aligned} \quad (4)$$

The eigenvectors show the relation between  $u(x, t)$  and  $\eta(x, t)$  in a each wave, e.g. in a right-going wave on constant depth,  $u(x, t) = +\sqrt{g/H} \eta(x)$ . This relation is equation (1) in Section 2 of the paper.

Now consider the wave form generated by a moving vertical wall at one boundary of the domain, which acts as a piston on the water. The linearization assumes the displacement of the wall is negligible relative to the length scale of interest, i.e. linearized about a fixed wall location, say at  $x = 0$ . If the horizontal wall velocity is  $U(t)$  and the still-water depth is  $H$ , then the horizontal fluid velocity has the same form as  $U(t)$  and propagates away from the wall with speed  $\sqrt{gH}$ . If the wall is at  $x = 0$ , then for  $x \geq 0$ :

$$u(x, t) = \begin{cases} U(t - x/\sqrt{gH}) & \text{if } x \leq \sqrt{gH} t, \\ 0 & \text{if } x > \sqrt{gH} t \end{cases} \quad (5)$$

The surface elevation  $\eta(x, t)$  is given by

$$\eta(x, t) = \sqrt{H/g} u(x, t) \quad (6)$$

which follows from the form of the eigenvectors. This is equation (5) in the text with slightly different notation.

### **Text S2. Numerical simulations.**

Figure 4 in the text shows numerical simulations of a simplified one-dimensional test case in which a basin with depth 200 m is connected to a river with depth 10 m or 1 m, with the waves induced by horizontal accelerations given by the seismic waveform shown in Figure 2. The implementation is described further in Section S3. Figure 4 shows the top few meters of the water only. For completeness, Figure S1 shows the full topography for the two cases shown in Figure 4.

In Figure S2 we show the full topography for two additional cases not shown in the main paper, and Figure S3 shows the simulation results. In these cases the vertical wall at the left boundary has been replaced by a somewhat more realistic sloping sea bed, reaching 200 m depth at 5 km from the shore at the left boundary. One might think that the tsunami waves generated in this case would have longer wavelength than in the case of a vertical wall. However, as a gentle slope moves back and forth the water surface rises and falls throughout this region, essentially returning to its original level if the net displacement is 0. This is not exactly true since waves start to propagate during this motion, but the net effect is that most of the waves cancel out. For the simplified topography shown in Figure S2, the waves that persist are those generated at the discontinuity in bottom slope at  $x = 5000$  m, giving two waves that move outward that are visible in the top plots of Figure S3 at  $t = 900$  seconds, and in the plots at  $t = 1020$  s as they reach the left

shore and river mouth, respectively. Their period is directly proportional to the temporal period of the oscillating seismic forcing and their spatial wavelength is this period scaled by the shallow water wave speed. This is exactly the same as what was observed for the case of a vertical wall.

Moreover, it is seen in the simulations of Figure S3 that the amplitude of the waves is considerably smaller than in the case of the vertical wall (Figure 4). This is because the total mass of water set into motion is the same in both cases, but on the gentle slope the vertical motion resulting from a given horizontal motion is smaller. There is also more cancellation of the positive and negative pulses and the remaining waves are smaller amplitude.

A more realistic seafloor that is not piecewise linear would give rise to more waves of smaller amplitude, which cancel out even more effectively in the situation where the net displacement by the end of the forcing is 0. From other simulations not shown here, it seems impossible to generate waves with longer wavelength or larger amplitude than what is seen in the case of a vertical wall, provided the seismic forcing is kept fixed.

Figure 4 and S3 show only a few frames of the simulation results. Animations are available as part of this SI for all four simulations shown in the figures:

**Caption for Movie S1.mp4.** Case 1 shown in Figure 4(a).

**Caption for Movie S2.mp4.** Case 2 shown in Figure 4(b).

**Caption for Movie S3.mp4.** Case 3 shown in Figure S3(a).

**Caption for Movie S4.mp4.** Case 4 shown in Figure S3(b).

**Text S3. GeoClaw software.** The simulations presented in Sections 4 and S2 were performed using the open source GeoClaw software that is distributed as part of Clawpack

(Clawpack Development Team, 2023). A pre-release version of Clawpack Version 5.10.0 was used, which includes a one-dimensional version of the GeoClaw code. [To be released soon, and this code is already available in the master branch of the code on Github.]

The primary modification needed for the simulations presented here was to incorporate the horizontal acceleration from the seismic signal. In reality the ground is moving, but computationally we work in the reference frame of the ground, assuming that the motion is spatially uniform over the small length scale of the simulation. With this assumption, the shallow water equations are solved on fixed topography but with the addition of a source term in the horizontal momentum equation that is the negative of the horizontal ground acceleration given by the synthetic seismogram. This same approach has been used in two space dimensions to study seismic seiching for other applications, both with GeoClaw and by other researchers using different software packages.

The complete implementation for the test cases shown here is available in the Github repository for this paper, <https://github.com/rjleveque/ChicxulubTanisSurge>.

This includes the seismic acceleration modifications and also the input data required for each case shown in the paper, along with Python scripts to perform the model runs and create the plots shown and the animations available as part of this SI.

## References

Clawpack Development Team. (2023). *Clawpack software*. <http://www.clawpack.org>.

doi: 10.17605/osf.io/kmw6h

LeVeque, R. J., George, D. L., & Berger, M. J. (2011). Tsunami modelling with adaptively refined finite volume methods. *Acta Numerica*, 20, 211 – 289. doi:

10.1017/S0962492911000043

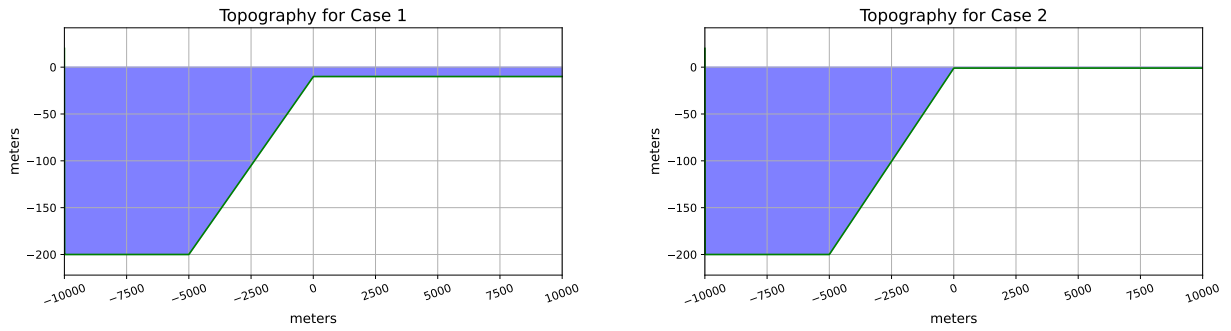


Figure S1. Topography for the two simulations shown in Figure 4.

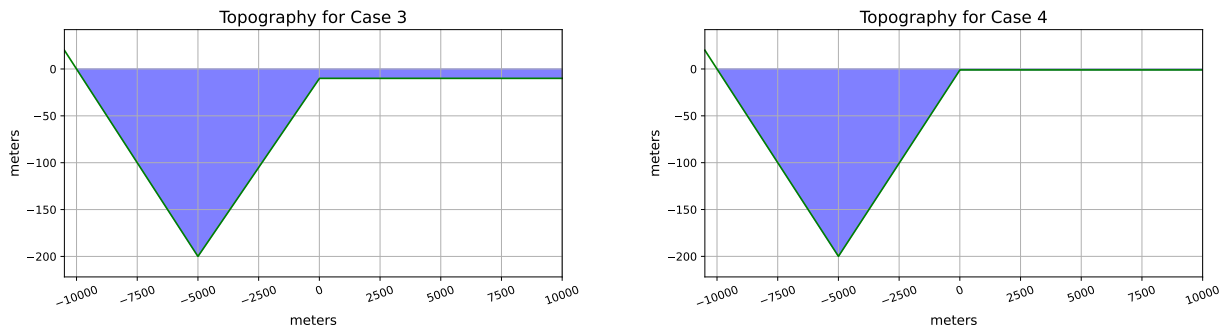
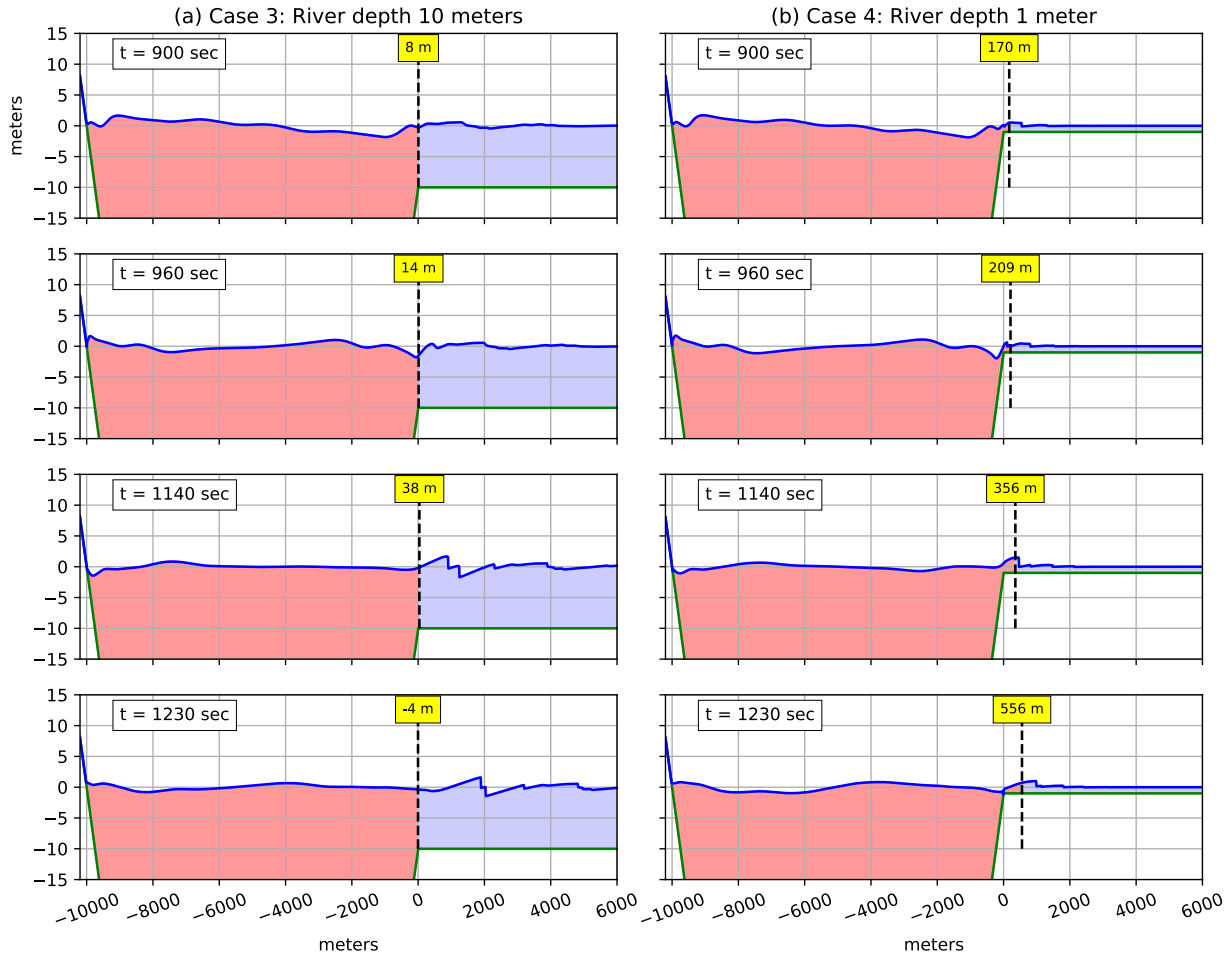


Figure S2. Topography for the two simulations shown in Figure S3.



**Figure S3.** Numerical simulations (using nonlinear shallow water equations) of the tsunami generated by the seismic signal shown in Figure 2 in a basin of depth 200 m bounded by a sloping sea bed on the left and a “river” on the right. The vertical dashed line shows the interface between saltwater to the left and freshwater to the right, and the distance from the river mouth at  $x = 0$  to this interface is noted in the attached box. (a) The left column is for a river depth of 10 m. (b) The right column is for a river depth of 1 m. The plots show only the upper 20 m of the basin. See Figure S2 for the full topography.